

Zone plate focused soft X-ray lithography for fabrication of nanofluidic devices

Adam F. G. Leontowich and Adam P. Hitchcock*

Brockhouse Institute for Materials Research,
McMaster University, Hamilton, ON, Canada L8S 4M1

ABSTRACT

Sealed nanofluidic channels with cross sections of sub-100 nm * 100 nm were created in a polymer bilayer using the focused soft X-rays of a scanning transmission X-ray microscope and the direct write method. The width of the nanochannels can be controlled by the area patterned in X and Y, while the height can be controlled by tuning the layer thicknesses. Formation of the desired structures has been confirmed by near edge X-ray absorption fine structure spectromicroscopy and scanning electron microscopy. The maximum length of the nanochannels fabricated by this method was found to be limited by the efficiency of excavation of patterned material out of the channel, as well as the stability of the polymer over-layer which seals it. Schemes toward interfacing these nanochannels with conventional microfluidics are discussed.

Keywords: nanofluidics, X-ray lithography, advanced lithography, zone plates, NEXAFS spectromicroscopy

*aph@mcmaster.ca; phone 1 905 525-9140 x24749; fax 1 905 521-2773

1. INTRODUCTION

Monochromatic zone plate focused X-rays offer the possibility of direct write lithography, analogous to lithography with a focused electron beam, using established electron beam resists and development procedures. Historically, the majority of this work has been performed using scanning transmission X-ray microscopes (STXM) operating at soft X-ray photon energies (100 – 2500 eV, 12 – 0.5 nm). The minimum feature size obtainable is steadily approaching that of focused ion or electron beams. Initial work by Zhang et al. (1995)¹ with the Stony Brook scanning transmission X-ray microscope at National Synchrotron Light Source (NSLS) reported feature sizes of 300 ± 20 nm in poly(methyl methacrylate) (PMMA), significantly worse than the quoted spot size of the instrument. Caster et al.² using hydrogen silsesquioxane (HSQ) as the resist, were able to achieve 90 ± 14 nm lines. Recently Leontowich et al.,³ working at 300 eV and much lower X-ray exposures, were able to achieve 40 ± 5 nm lines in PMMA. The demonstrated feature size here was quite close to the Rayleigh resolution limit dictated by the properties of the zone plate lens used.

Patterning with monochromatic soft X-rays with full control over the photon energy, and a band width better than 0.2 eV, has opened up a unique patterning technique for multilayer resists that we have termed “chemically selective patterning”. The concept is as follows: Different molecules containing different elements or chemical functional groups often display different X-ray absorption spectra. Most resist-type molecules (polymers) experience chemical changes when irradiated with X-rays which can then be probed by X-ray absorption spectroscopy.⁴⁻⁶ If the sufficiently monochromatic X-ray beam is tuned to a photon energy corresponding to an absorption resonance exclusive to one component, then one can induce a chemical change to that component nearly independently of the others at the same point on the sample by patterning at that energy. Modern STXMs on synchrotron beamlines exceed the system requirements necessary to realize this concept. Using the Advanced Light Source (ALS) STXM 5.3.2.2, Wang et al. demonstrated chemically selective patterning of bilayer⁷ and later trilayer⁸ samples.

In this report we have combined chemically selective patterning of polymer multilayer samples with a suitable development procedure in order to demonstrate in a proof of concept experiment fabrication of nanofluidic (sub-100 nm) channels with the tunable, focused soft X-rays of a STXM. The restrictions on materials, patterning, developers, etc. for

this technique, and the underlying mechanisms of nanochannel formation are discussed. A potentially functional nanofluidic device is presented, and schemes to interface such devices with conventional microfluidics to realize fully functional fluidic devices are described.

2. METHODOLOGY

2.1 Appropriate resists for chemically selective lithography

2.1.1 Controlling the location of energy absorption by chemically selective patterning

Only those samples which fit the criteria outlined in this report may be suitable for chemically selective patterning with a STXM. The foremost sample requirement is that it must contain at least two chemically different components, and each component must display a significantly different X-ray absorption spectrum over a chosen photon energy region. Ideally, the spectrum of each component molecule should have a large inner shell resonance at a chosen absorption edge, and these resonances should be separated in energy by more than their feature width, i.e. by 1 eV or more. The absorption edge must also be within the energy range achievable by the beamline (100 – 2500 eV for existing soft X-ray STXM beamlines; 270 – 580 eV for ALS STXM 5.3.2.2 where this work was performed). The photon energy is then tuned to those specific resonance energies of the sample when patterning, so that the rate of energy absorption by one component is significantly greater than the other and vice versa. In principle the components could be selected based on different elemental composition (i.e. one component could contain F but not N, while the other contains N but not F) but in practice patterning at one absorption edge is preferred as moving between absorption edges often requires re-optimization of the STXM and beamline which may compromise the spatial alignment of multiple patterns. In addition, higher energy edges such as the N 1s edge, have a significant underlying absorption from the C 1s ionization continuum which is common to all molecules containing C.

Wang et al.^{7,8} showed experimentally that differing X-ray absorption cross sections and a monochromatic beam are not sufficient to realize chemically selective patterning. The concept only succeeded when applied to vertically-segregated multilayer structures, rather than phase separated blends or homogeneous material with multiple chemical functional groups sharing the same polymer backbone, or within the monomeric repeat unit. The mechanism put forth by Wang to explain the success of the layered structure has since been proven incorrect by Leontowich,³ and a new mechanism to explain the successful patterning of only layered samples is proposed here: When one component is selectively irradiated with soft X-rays, it initiates a cascade of damaging secondary processes, the dominant process being generation of secondary electrons (photoelectrons, Auger, shake-off, shake-up, etc.). The initial photoabsorption of energy can be made specific by tuning the patterning photon energy to an absorption resonance exclusive to one component, however, the damaging secondary processes are not specific. The specificity is lost if both components are within the damaging radius of the secondary processes. In a layered sample, there can be sufficient spatial separation of the absorbing and non absorbing components of the sample if enough of the non-resonant layer lies outside the damaging radius of the secondary processes emitted by the resonant layer, which typically have a range of a few nm at soft X-ray photon energies.⁹ This distance sets a minimum layer thickness for which chemically selective patterning will succeed, which we estimate to be 20 nm. The maximum total thickness of all layered components can only be about 300 nm to avoid absorption saturation.

2.1.2 Added requirements for chemically selective lithography

A development step which often consists of dipping the sample in a suitable solvent to reveal the patterned areas is necessary to realize nanofluidic channels or other unique structures, and differentiates chemically selective patterning^{7,8} from the present approach of chemically selective lithography. The solubility of the components of the multilayer sample in the developer must be taken into consideration. If for example, a bilayer is made of two components which both act as positive resists (irradiated material is removed by developer, non-irradiated material is unaffected), then the developer for the top layer can not significantly attack/dissolve the non-irradiated portions of the bottom layer and vice versa, or the structure would be ruined. This is perhaps the most inflexible requirement of chemically selective lithography. As one uses more layers of different components (beyond two) it becomes increasingly difficult to find polymeric components with both the appropriate X-ray absorption properties and suitable orthogonal developers.

2.2 Sample preparation

The samples in this report consist of a 30 – 100 nm layer of poly(dimethylglutarimide) (PMGI, a gift from Prof. Ash Parameswaran, Simon Fraser University, British Columbia, Canada), on a 30 – 100 nm layer of poly(methyl methacrylate) (PMMA, electronics grade, 315,000 M_w , 1.05 M_w/M_n , Polymer Source Inc.), on a Si_3N_4 window (75 nm * 1 mm * 1 mm window area in a 200 μm * 5 mm * 5 mm Si frame, Norcada Inc.). PMMA layers were fabricated by spin casting 1.0 – 2.0% w/w solutions of PMMA in toluene (99.9% Chromasolv®, Sigma-Aldrich) onto freshly cleaved mica (Ted Pella Inc.). The layer on mica was scribed into 3 * 3 mm pieces with scalpel, and slowly dipped into a Petri dish of distilled water. Pieces of the film detach from the mica and float upon the waters' surface, and one piece was then caught on a Si_3N_4 window in an orientation which partially covered the window to allow for measurements of the spectrum of incident radiation (I_0) later on. The sample was then annealed for 1 hour at 150 °C at reduced pressure ($\sim 2 * 10^{-2}$ Torr). Next, layers of PMGI were fabricated by spin casting 1.0 – 2.0% w/w solutions of PMGI in *N, N*-dimethylformamide (99.9% Chromasolv®, Sigma-Aldrich) onto freshly cleaved mica. The PMGI layer on mica was then annealed for 5 minutes at 230 °C. One 3 * 3 mm piece of PMGI was transferred onto the sample by the float method above in an orientation that partially covered the PMMA layer yet only partially covered the window. This multiple float procedure has opened up greater possibilities for samples than our previous multiple spin casting procedure.^{7,8} Finally, the sample was annealed for 15 minutes at 150 °C at reduced pressure ($\sim 2 * 10^{-2}$ Torr).

2.3 Scanning transmission X-ray microscope (STXM)

Patterning of samples, collection of near edge X-ray absorption fine structure (NEXAFS) spectra, and imaging was performed with the STXM¹⁰ at beamline 5.3.2.2¹¹ at the Advanced Light Source (ALS), Lawrence Berkeley National Laboratories (LBNL). Zone plate lenses were supplied by the Center for X-ray Optics (CXRO) with the following parameters: 25 nm outer most zone width, 240 μm diameter, 90 μm central stop. A 50 μm order sorting aperture was used to suppress higher order light, as well as a 1 m long section of beamline differentially pumped with 0.6 Torr of N_2 . Experiments were performed with the STXM chamber backfilled with 250 Torr He, after the evacuation of air. Entrance (50 μm) and exit (25 * 25 μm) slit settings were chosen so that focusing performance would be diffraction-limited, offering the smallest possible spot size.¹²⁻¹⁴ Details of the pattern generation program and the calculation of doses, which are believed to be precise within 10%, have been reported previously.^{3,7,8}

2.4 Development

A 7:3 2-propanol (IPA, 99.5%, Caledon) : H_2O solution was used as the developer for PMGI,¹⁵ while a 3:1 IPA : 4-methyl-2-pentanone (MIBK, >98.5% ACS reagent grade, Sigma-Aldrich) solution was used to develop the PMMA layer.¹⁶ The performance of both developer/resist systems for this application has been explored previously.³ To develop, a sample was held with locking tweezers, then fully immersed in a vial containing the PMGI developer solution and gently stirred for 10 s. The sample was then immediately immersed into a waiting vial containing the PMMA developer solution and stirred for 30 s. Afterward, the sample was allowed to dry in ambient air. All development occurred at ambient temperature (~ 20 °C). These specific development times and conditions were applied for all results presented in this report.

2.5 Imaging

Optical micrographs of samples were collected using an Olympus BX51 optical microscope equipped with a CCD camera. The nanofluidic structures were imaged by three techniques, atomic force microscopy (AFM, Quesant 350 microscope, Budget Sensors Tap150Al-G probes, tapping mode), NEXAFS spectromicroscopy (section 2.3), and scanning electron microscopy (SEM, JEOL JSM-7000F microscope, 10 keV, 60 μA beam current, working distance: 5 mm). A 5 ± 1 nm Pt layer was applied (682 Precision Etching Coating System, Gatan) prior to SEM imaging to reduce charging and improve contrast. It is imperative to image the structures in the proper order to avoid introducing artefacts. Both SEM and STXM involve ionizing radiation which can induce mass loss, chemical changes, and deposit carbon,¹⁷ permanently altering the sample.⁴⁻⁶ Tapping mode AFM imaging did not noticeably alter the sample and therefore was always performed before SEM or STXM imaging. Identical duplicate structures were made on separate samples to obtain artefact free SEM and STXM images of the same structure.

3. RESULTS

3.1 Layered structure and NEXAFS spectra

An optical micrograph of a PMGI/PMMA/Si₃N₄ sample is presented in Figure 1a. C 1s (K) NEXAFS spectra were collected from areas of this sample composed only of one of the layers. These spectra were normalized to 1 nm thickness of material using the elemental response for the formula repeat unit,¹⁸ and the known bulk densities. The normalized spectra are presented in Figure 1b. The spectrum of PMGI is dominated by the large C 1s(C=O) → π*_{C=O} absorption feature at 287.7 eV, while the spectrum of PMMA is dominated by a slightly larger C 1s(C=O) → π*_{C=O} absorption feature at 288.5 eV. The π*_{C=O} resonance of PMGI is red shifted by 0.7 eV relative to PMMA due to differences in the electronic environment surrounding the carbonyl bond.¹⁹

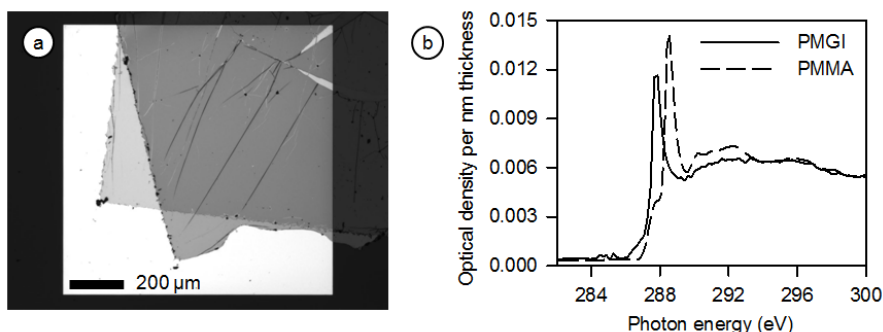


Figure 1: a) Optical micrograph of a PMGI/PMMA/Si₃N₄ sample. b) X-ray absorption (NEXAFS) spectra of PMGI and PMMA, normalized to 1 nm thickness.

3.2 Fabricating nanochannels

Two pattern generation files, each consisting of sets of discrete points on a 30 nm rectilinear grid, were created to fabricate nanochannels. Pattern A (Figure 2a) consisted of two parallel 570 * 570 nm square areas (i.e. 19 x 19 point exposures) separated by 4000 nm, while pattern B (Figure 2b) consisted of a 4680 nm long, 90 nm wide area. A graphical representation of the final desired structure and its orientation relative to the incident X-ray beam is presented in Figure 2c.

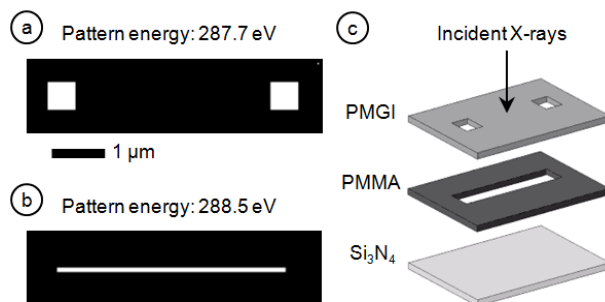


Figure 2: a) Pattern A; access hole pattern for the top PMGI layer. b) Pattern B; channel pattern for the bottom PMMA layer. c) Exploded view drawing of the desired nanofluidic structure. a) and b) are on the same positional scale.

A region of the PMGI/PMMA bilayer was then brought into sharp focus in the STXM, and was subsequently chemically selectively patterned in the following manner: The photon energy was tuned to 287.7 eV and pattern A was executed using the PatternGen routine³ in the STXM_control program with precise dwell time and sample position control (better than 10 nm by laser interferometry¹⁰). After completion, the photon energy was tuned to 288.5 eV and pattern B was executed over the exact same area as pattern A. Several combined A B patterns were made on the same sample covering

a range of dwell times. The sample was then removed from the STXM chamber and developed (section 2.4). The developed samples were loaded into the STXM chamber, and imaged at 288.5 eV (Figure 3). Figures 3a – e are STXM optical density (OD) images of developed patterns generated with successively increasing exposure times (2 – 5 ms) corresponding to increasing doses (1 – 3 MGy) for pattern B, while the exposure times for pattern A were held constant (14 ms, 10 MGy).

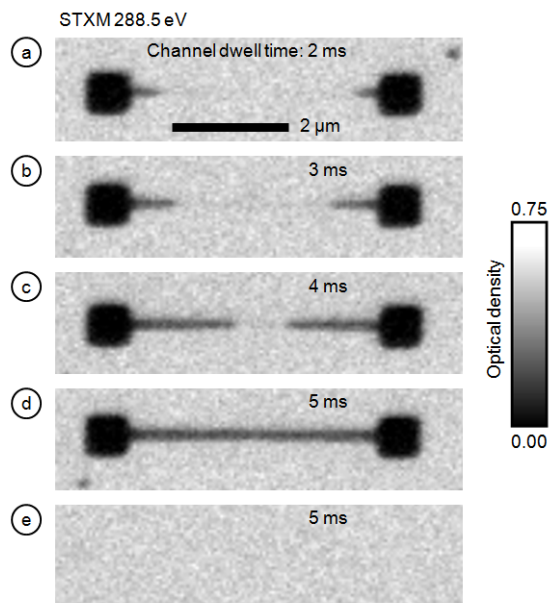


Figure 3: STXM OD images at 288.5 eV of developed PMGI/PMMA/Si₃N₄ samples patterned with different exposure times for the channel (a = 2 ms, b = 3 ms, c = 4 ms, d = 5 ms, e = 5 ms). Exposure time for the access holes for a – d was 14 ms. Access holes were not patterned for e). With a sufficient dose (3 MGy), the channel is fully cleared by the developer, if access holes are present. All images are on the same positional and OD scale.

The patterned PMMA material in the nanochannel is removed beginning from the square areas of pattern A (i.e. access holes) inward. As the dose received by the PMMA in the nanochannel area increases the nanochannel is developed further underneath the PMGI layer. The dose received by the patterned PMMA material in the nanochannel in Figure 3d was enough that it could be fully cleared during development. In Figure 3e, pattern B was executed with the same dwell time/dose as Figure 3d, but here pattern A was not executed; enough dose was given to clear the nanochannel, yet in this case the patterned material in the nanochannel was not removed during development.

3.3 Characterization of the nanochannel

A C 1s image sequence (or stack²⁰) of the nanochannel structure of Figure 3d was collected with the STXM. The stack, which consists of a C 1s NEXAFS spectrum for every pixel in an imaged area, was fit to the normalized PMGI and PMMA reference spectra (Figure 1b) using singular value decomposition (SVD) routines²¹ implemented in aXis2000.²² Figure 4 displays the resulting *quantitative* PMGI (Figure 4a) and PMMA (Figure 4b) component maps along with a color coded composite (Figure 4c). Since the NEXAFS spectra used for the fit procedure are normalized to 1 nm material, the component maps are literally thickness maps of each component in the system. As there are only two components here (PMGI and PMMA) the fit is very good and allows an accurate ($\pm 5\%$) determination of the thickness of each layer at every pixel. The total thickness of the bilayer derived from the individual component maps is consistent with data from an AFM image of the structure (not shown), within measurement uncertainties. The thickness of the PMMA layer within the nanochannel area is equal to that of the developed access hole areas, based on SVD analysis of the C 1s NEXAFS spectrum of the nanochannel. This indicates that the patterned PMMA in the nanochannel area has been practically fully removed by the developer. The thickness of the PMGI layer in the area of the nanochannel, which serves to seal it, is slightly different from elsewhere on the film; there was loss of $20 \pm 5\%$ of the PMGI top layer in the patterned nanochannel area. An SEM image was also taken of the nanochannel structure of Figure 3d and is presented in

Figure 4d. The morphology of the square areas is consistent with that of bare Si_3N_4 , and despite some loss of PMGI material the layer sealing the nanochannel appears intact and free of pinholes.

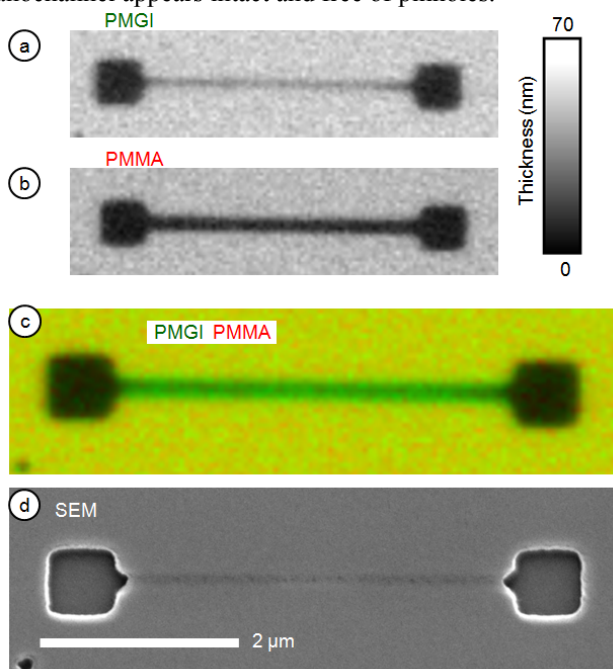


Figure 4: Quantitative component maps of a) PMGI and b) PMMA derived from SVD analysis of NEXAFS spectromicroscopy data, on the same positional and thickness scales. c) Non rescaled two color composite map of a) in green, and b) in red. Yellow corresponds to the presence of both polymer layers. d) Scanning electron micrograph of the nanochannel structure. c) and d) are on the same positional scale.

3.4 Optimizing doses and development times

SEM images collected at a 45° tilt of developed nanochannel structures are presented in Figure 5. The dwell time/dose to the channel in Figure 5a is the same as Figures 3d and 4. The entrance to the nanochannel is clearly observed, as well as the defect free PMGI top layer. SEM images of nanochannel structures fabricated with increased doses are presented in Figures 5b and 5c. As the dose is increased, pinhole defects in the PMGI top layer are observed, and eventually this covering layer is fully removed. Thus under the conditions presented, a “dose window” between 2.5 – 3.5 MGy exists in which the patterned PMMA in the nanochannel can be fully cleared while the top PMGI remains free of pinhole defects, sealing the channel.

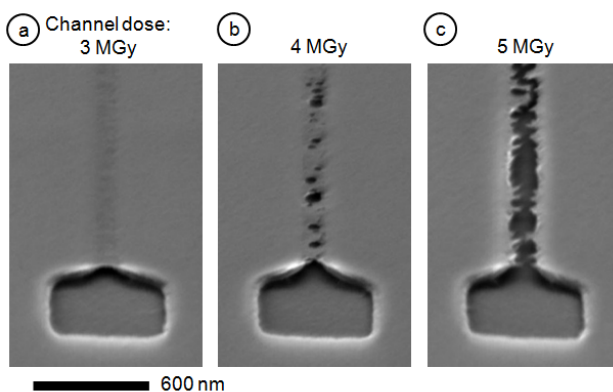


Figure 5: Scanning electron micrographs of nanochannels tilted at 45° fabricated by chemically selective lithography. a) Under optimal dose conditions (3 MGy), the channel is cleared yet the PMGI overlayer remains intact. b) Pinholes appear at channel doses >3.5 MGy, or c) the PMGI overlayer is fully removed. All images are on the same positional scale.

The development time for both PMGI and PMMA developers was also optimized. To reduce the removal of the PMGI layer sealing the nanochannel the amount of time the sample spends in PMGI developer should be as short as possible. It was found that the development time could be reduced to 10 s from the recommended time of 60 s¹⁵ if the dwell time for pattern A was increased. Here the increased dwell time was acceptable as both layers in the patterned area need to be fully removed to the substrate, although a larger increase in dwell time will result in rounded edges and expanded access holes (section 4.3). It is also conceivable that the amount of time the sample spends in PMMA developer should be as long as possible to increase the maximum nanochannel length. PMMA development times of 30 s, 60 s and 120 s were tested, but it was found that the 60 s and 120 s only increased the number and size of pinholes in the PMGI layer covering the nanochannel, therefore 30 s was optimal.

3.5 Cross sectional area of the nanochannel in relation to its maximum length

The pattern generation files were modified to explore the effect of a wider patterned channel area on its developed length. One 570 * 570 nm square was deleted from pattern A, and the length of pattern B was increased to 30 μm, while the width was varied (60, 90, 150, and 210 nm). Patterning of the sample was carried out as previously described. The dwell time/pixel (5 ms) was constant for all modified pattern B channel patterns, as well as the modified pattern A (14 ms), respectively. The patterned samples were then developed and imaged by STXM and AFM (Figure 6).

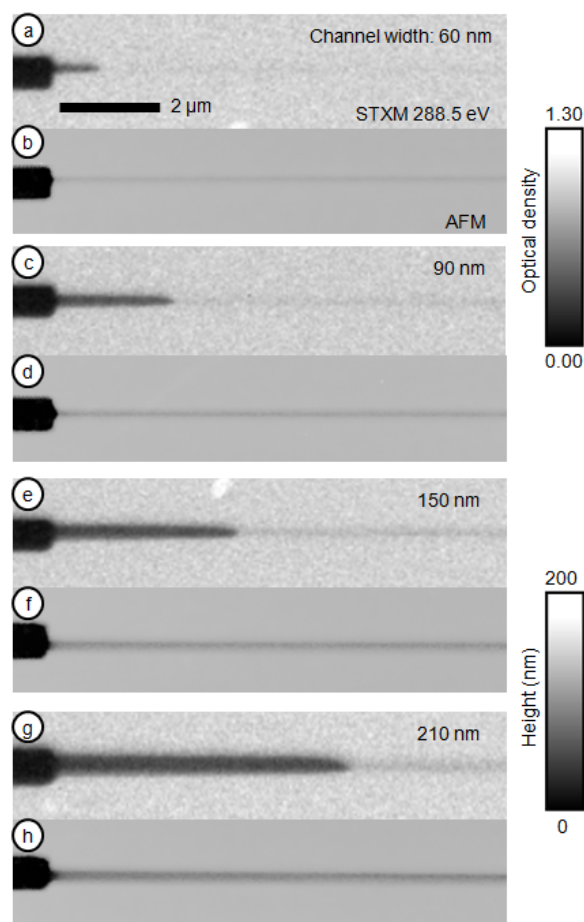


Figure 6: STXM OD and AFM images of nanochannels created with the same dwell time (5 ms) but different width. STXM and AFM images are on the same OD and Z scale, respectively, and all are on the same positional scale.

The STXM OD images show that as the width of the patterned nanochannel is increased, its developed length increases. AFM images reveal the entire nanochannel area patterned undergoes a decrease in height. A cross comparison with the STXM OD images reveals that the height reduction is the same whether the patterned PMMA material underneath is

removed or not. This result suggests that the thickness reduction is due to removal of PMGI during development, rather than the sagging of the PMGI top layer over the nanochannel, which is in agreement with the NEXAFS spectromicroscopy PMGI component map.

Although the same dwell times were used for all nanochannel patterns (pattern B) in Figure 6, the dose for the wider channels is not precisely the same as that of the narrower channels. The intense spot of focused X-rays at the focal plane is a distribution (often showing side lobes¹⁴, characteristics of being diffraction limited^{12,13}) rather than a finite circle, thus there is a cumulative dose overlap from adjacent exposures and as a result the material at the center of the channel receives a higher dose than that at the edges. However, a conceptually analogous experiment yielded an identical result. The height of the nanochannel is dependent upon the thickness of the bottom layer, which can be fine-tuned by adjusting the concentration of polymer solution before spin casting; increasing the thickness of the bottom PMMA layer increases the cross sectional area of the nanochannel. With a thin layer of PMMA (40 nm), the maximum length that a 90 nm wide nanochannel could be fully cleared yet free of pinholes is $5 \pm 1 \mu\text{m}$. With a thicker layer of PMMA (90 nm), this distance increased to $8 \pm 1 \mu\text{m}$.

4. DISCUSSION

4.1 Maximum nanochannel length

Patterning of the nanochannel was performed at 288.5 eV, corresponding to the maximum absorption cross section of PMMA at the C 1s edge. The energy absorption rate of PMMA at this photon energy is significantly greater than that of PMGI allowing its selective patterning. However, PMGI also absorbs energy, albeit at a lower rate, because the absorption cross section of PMGI at 288.5 eV is not zero (Figure 1b). This residual dose into the PMGI top layer during patterning of the nanochannel is enough to cause partial removal of the PMGI top layer, as observed by NEXAFS spectromicroscopy (Figure 4) and AFM (Figure 6). Within an experimentally determined dose window, this process is insignificant overall as PMGI remains continuous and seals the nanochannel. But at higher dwell times the residual dose induces significant pinhole formation, and eventually results in the full removal of the PMGI layer as well. This imposes an upper limit on the dwell time for patterning the nanochannel, even when done chemically selectively.

To realize the nanochannel, the PMMA developer solution must diffuse under the PMGI layer, into the nanochannel, dissolve the patterned PMMA material, and then diffuse out. When PMMA is exposed to ionizing radiation at low dose it primarily undergoes main chain scission which decreases the molecular weight and dramatically increases solubility in the PMMA developer solution.¹⁶ The development/excavation process of the patterned PMMA material in the nanochannel can therefore be facilitated by increasing the dose to the nanochannel, but only up to the limit imposed by the pinhole formation in the PMGI layer. The maximum length of the channel then becomes dependent upon the diffusion of developer into and out of the nanochannel. The longer the channel is, the more difficult excavating the patterned material inside the channel becomes. The diffusion limited excavation can be aided by increasing the cross sectional area of the nanochannel. When the cross sectional area is increased, conceivably better flow occurs, and longer nanochannels were realized. Consequently, this gets away from the uniqueness of our approach as the nanochannels take on larger dimensions. The maximum length that a $100 * 100 \text{ nm}$ nanochannel could be fabricated without pinholes was $10 \pm 1 \mu\text{m}$.

4.2 Interfacing with conventional microfluidics

The nanochannels fabricated here should be viable for working fluidic devices. The impermeability of the PMGI overlayer sealing the nanochannel is demonstrated in Figure 3e. Here only pattern B was carried out at the dose required to clear the nanochannel. Without defined “access holes”, either the developer could not reach the patterned PMMA or the solvated material could not escape (or a combination of these two effects) and the nanochannel was not realized. Work on functioning fluidic devices has begun. Images of a double T injector test structure fabricated with STXM 5.3.2.2 are presented in Figure 7. A major challenge now is plumbing this device so that the flow of liquid in and out can be controlled, and the velocity and flow rate measured, etc. We are attempting to interface this structure with more conventional microchannels by ‘bonding’ a poly(dimethylsiloxane) (PDMS) chip on top of the structure.²³ To that end, the access holes have been extended to a length of $50 \mu\text{m}$ to ease the alignment when mating the two structures.

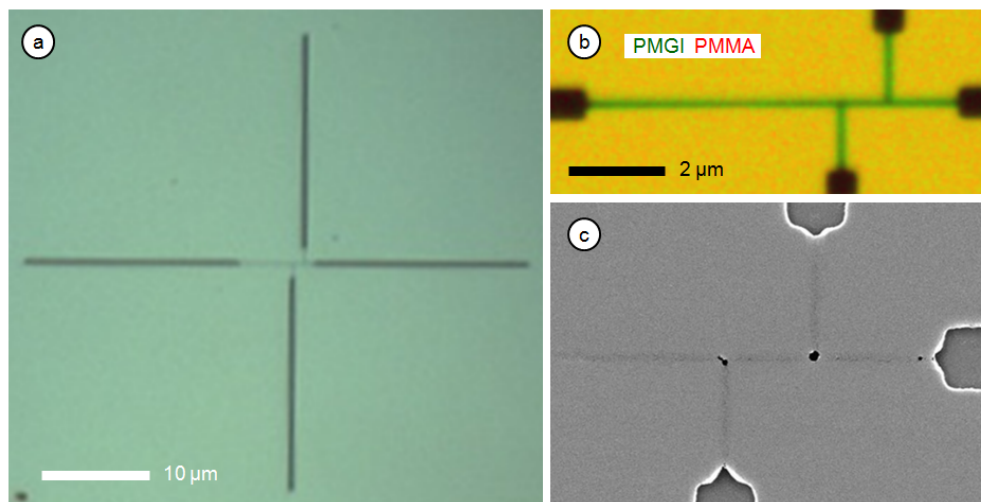


Figure 7: A double T injector device fabricated by chemically selective lithography. a) Optical micrograph (100x, reflection) of the entire device. b) Non rescaled two color composite map (PMGI in green, PMMA in red) derived from SVD analysis of NEXAFS spectromicroscopy data. c) Scanning electron micrograph of the device. Pinholes occurred at the intersections of channels.

4.3 Outlook

The survival of the top PMGI layer was a major challenge in this project. Here the absorption cross sections of the two components were just different enough to be viable but it would be beneficial if the difference in X-ray absorption was much larger. Furthermore the orthogonal developer requirement imposes limits which will probably make it difficult to evolve to completely three dimensional fluidic structures. Perhaps a better approach would be to use one resist with different initiator molecules such as photoacid generators²⁴ in layers which would bypass the need for orthogonal developers for each layer. Use of a self developing resist²⁵ would alleviate both the orthogonal developer and diffusion issues. Moving to higher X-ray photon energies may allow patterning and fabrication of thicker, more complex structures as photoabsorption cross sections decrease with increasing photon energy, reducing absorption saturation. However, the damaging radii of secondary processes increases; the inelastic mean free path, and the significance of fluorescence increase with higher photon energy. The soft X-ray region appears best suited to this type of approach.

This is a proof of concept demonstration for the formation of nanochannels by chemically selective lithography. For a functional nanofluidic device, the materials of the structure must ultimately be compatible with the solvent and analyte molecules. Although not yet tested, these PMGI/PMMA/Si₃N₄ nanochannels should be compatible with water and mild buffer solutions with a pH near 7.

Direct write patterning in STXM would benefit from a point spread function¹⁴ correction program, which would calculate the cumulative dose overlap from adjacent exposures and adjust the dwell time for each pixel to correct for it. For example, the holes seen only at the nexus of the nanochannels (Figure 7c) are likely due to overlap of point spread functions. Solutions to this problem exist for electron beam lithography²⁶ but have yet to be applied to patterning in STXM. Integrating a point spread function correction into the pattern generation program should increase the homogeneity of dose providing uniform exposure for complex patterns.

Finally, the concept of chemically selective lithography (section 2.1) is not exclusive to the direct write method, which is not well suited to the photolithographic mass production of devices. Multiple patterned masks, one for each layer/photon energy, could be fabricated and exposed with a suitable monochromatic beam for full wafer production. The exposures would need to be precisely aligned, but development of this technology is well underway within the deep X-ray lithography community.²⁷ The necessity of bright, tunable soft X-rays precludes a synchrotron source, therefore the experiment would essentially require mating an X-ray lithography scanner endstation with multiple patterning ability with a soft X-ray beamline at a synchrotron facility.

5. CONCLUSION

Sealed nanochannels with dimensions on the order of sub-100 nm were created in polymer bilayers with tunable focused soft X-rays and the direct write method. For a 100 x 100 nm channel, the maximum nanochannel length realized was $10 \pm 1 \mu\text{m}$. Excavation of the patterned channel material was found to be the largest impediment to the realization of even longer channels. If the cross sectional area is increased, a longer channel can be realised.

ACKNOWLEDGEMENTS

This research was supported by NSERC (Canada), the Canada Foundation for Innovation and the Canada Research Chair program. Adam Leontowich acknowledges receipt of an ALS Doctoral Fellowship in Residence. We thank Prof. Ash Parameswaran for the poly(dimethylglutarimide) and Prof. Dongqing Li for useful discussion of interfacing nanofluidics. We also thank Dr. David Kilcoyne and Dr. Tolek Tyliczszak for their support of the STXM facilities. The experiments were performed at the Advanced Light Source, beamline 5.3.2.2 (ALS, Berkeley, CA, USA). The Advanced Light Source is supported by the Director, Office of Energy Research, Office of Basic Energy Sciences, Materials Sciences Division of the U.S. Department of Energy, under Contract No. DE-AC03-76SF00098.

REFERENCES

- [1] Zhang, X., Jacobsen, C., Lindaas, S., and Williams, S., "Exposure strategies for polymethyl methacrylate from in situ x-ray absorption near edge structure spectroscopy," *J. Vac. Sci. Technol. B* 13, 1477-1483 (1995).
- [2] Caster, A. G., Kowarik, S., Schwartzberg, A. M., Leone, S. R., Tivanski, A., and Gilles, M. K. "Quantifying reaction spread and x-ray exposure sensitivity in hydrogen silsesquioxane latent resist patterns with x-ray spectromicroscopy," *J. Vac. Sci. Technol. B* 28, 1304-1313 (2010).
- [3] Leontowich, A. F. G., and Hitchcock, A. P., "Zone plate focused soft X-ray lithography," *Appl. Phys. A* 103, 1-11 (2011).
- [4] Coffey, T., Urquhart, S. G., and Ade, H., "Characterization of the effects of soft x-ray irradiation on polymers," *J. Elec. Spec. Relat. Phenom.* 122, 65-78 (2002).
- [5] Wang, J., Morin, C., Li, L., Hitchcock, A. P., Scholl, A., and Doran, A., "Radiation damage in soft x-ray microscopy," *J. Elec. Spec. Relat. Phenom.* 170, 25-36 (2009).
- [6] Wang, J., Botton, G. A., West, M. M., and Hitchcock, A. P., "Quantitative evaluation of radiation damage to polyethylene terephthalate by soft X-rays and high-energy electrons," *J. Phys. Chem. B* 113, 1869-1876 (2009).
- [7] Wang, J., Stöver, H. D. H., Hitchcock, A. P., and Tyliczszak, T., "Chemically selective soft X-ray patterning of polymers," *J. Synchrotron Rad.* 14, 181-190 (2007).
- [8] Wang, J., Stöver, H. D. H., and Hitchcock, A. P., "Chemically selective soft X-ray direct-write patterning of multilayer polymer films," *J. Phys. Chem. C* 111, 16330-16338 (2007).
- [9] Seah, M. P., and Dench, W. A., "Quantitative electron spectroscopy of surfaces: A standard data base for electron inelastic mean free paths in solids," *Surf. Interface Anal.* 1, 2-11 (1979).
- [10] Kilcoyne, A. L. D., Tyliczszak, T., Steele, W. F., Fakra, S., Hitchcock, P., Franck, K., Anderson, E., Harteneck, B., Rightor, E. G., Mitchell, G. E., Hitchcock, A. P., Yang, L., Warwick, T., and Ade, H., "Interferometer-controlled scanning transmission microscopes at the advanced light source," *J. Synchrotron Rad.* 10, 125-136 (2003).
- [11] Warwick, T., Ade, H., Kilcoyne, D., Kritscher, M., Tyliczszak, T., Fakra, S., Hitchcock, A., Hitchcock, P., and Padmore, H., "A new bend-magnet beamline for scanning transmission x-ray microscopy at the advanced light source," *J. Synchrotron Rad.* 9, 254-257 (2002).
- [12] Attwood, D., [Soft X-rays and Extreme Ultraviolet Radiation: Principles and Applications], Cambridge University Press, Cambridge (1999).
- [13] Hawkes, P. W., and Spence, J. C. H., [Science of Microscopy], Springer, New York, ch. 13 (2007).
- [14] Leontowich, A. F. G., Tyliczszak, T., and Hitchcock, A. P., "Measurement of the point spread function of a soft X-ray microscope by single pixel exposure of photoresists," *Proc. SPIE* 8077, 80770N-1 (2011).
- [15] Johnstone, R. W., Foulds, I. G., Pallapa, M. V., and Parameswaran, A. M., "Isopropanol/water as a developer for poly(dimethylglutarimide)," *J. Micro/Nanolithogr. MEMS MOEMS* 7, 043006 (2008).
- [16] Greeneich, J. S., "Developer characteristics of poly-(methyl methacrylate) electron resist," *J. Electrochem. Soc.* 122, 970-976 (1975).

- [17] Leontowich, A. F. G., and Hitchcock, A. P., "Secondary electron deposition mechanism of carbon contamination," *Appl. Phys. Lett.* submitted (2012).
- [18] Henke, B. L., Gullikson, E. M., and Davis, J. C., "X-ray interactions: Photoabsorption, scattering, transmission, and reflection at $E = 50\text{-}30,000$ eV, $Z = 1\text{-}92$," *Atom. Data Nucl. Data Tables* 54, 181-342 (1993).
- [19] Urquhart, S. G., and Ade, H., "Trends in the carbonyl core (C 1s, O 1s) $\rightarrow \pi^*_{\text{C=O}}$ transition in the near edge x-ray absorption fine structure spectra of organic molecules," *J. Phys. Chem. B* 106, 8531-8538 (2002).
- [20] Jacobsen, C., Wirick, S., Flynn, G., and Zimba, C., "Soft X-ray spectroscopy from image sequences with sub-100 nm spatial resolution," *J. Microscopy* 197, 173-184 (2000).
- [21] Ade, H., and Hitchcock, A. P., "NEXAFS microscopy and resonant scattering: Composition and orientation probed in real and reciprocal space," *Polymer* 49, 643-675 (2008).
- [22] aXis2000 is written in Interactive Data Language (IDL). It is available free for non-commercial use from <http://unicorn.mcmaster.ca/aXis2000.html>
- [23] McDonald, J. C., and Whitesides, G. M., "Poly(dimethylsiloxane) as a material for fabricating microfluidic devices," *Acc. Chem. Res.* 35, 491-499 (2002).
- [24] Pawloski, A. R., and Nealey, P. F., "Efficiency of photoacid generators in chemically amplified resists for 157nm lithography," *J. Photopolymer Sci. Tech.* 15, 731-740 (2002).
- [25] Ito, H., and Wilson, C. G., "Chemical amplification in the design of dry developing resist materials," *Polym. Eng. Sci.* 23, 1012-1018 (1983).
- [26] Pavkovich, J. M., "Proximity effect correction calculations by the integral equation approximate solution method," *J. Vac. Sci. Technol. B* 4, 159-163 (1986).
- [27] Schmidt, A., Ehrfeld, W., Lehr, H., Müller, L., Reuther, F., Schmidt, M., and Zetterer, Th., "Aligned double exposure in deep X-ray lithography," *Microelec. Eng.* 30, 235-238 (1996).